applied sciences

MDPI

Article

Real Stiffness and Fatigue Resistance of Stringer-to-Cross-Girder Connection of Riveted Steel Railway Bridges

Jozef Gocál [1,*], Josef Vičan [1] and Jozef Jošt [2]

[1] Department of Structures and Bridges, Faculty of Civil Engineering, University of Žilina, Univerzitná 8215/1, 010 26 Žilina, Slovakia
[2] Strength, s.r.o., Dlhá 88B, 010 09 Žilina, Slovakia
* Correspondence: jozef.gocal@uniza.sk

Abstract: Steel girder bridges with member decks belong to the most frequently used types of superstructures of old riveted steel railway bridges. During their service life, the bridge deck members are affected by escalating effects of the traffic loads that significantly exceed those for which they were originally designed. As a result, these structures are often subject to the increased effects of fatigue degradation. One of the typical cases of fatigue damage on steel riveted bridges is a fatigue crack in the web of the stringer at the point of its connection to the cross girder. Such a connection used to be considered to transmit the axial and shear forces only, and so no fatigue crack was expected to develop in this detail during the bridge service life. However, the relatively frequent occurrence of fatigue cracks indicates the incorrectness of this assumption. This article is divided into two parts. Firstly, the bending stiffness of the stringer-to-cross-girder connection with different structural arrangements is analysed. Theoretical and experimental analyses of fictitious steel superstructures as well as of a real superstructure of an existing steel riveted bridge were performed to clarify the real stiffness behaviour of this detail. The results of the analyses confirm the assumption of a certain bending stiffness of the observed connection. Subsequently, attention is paid to the fatigue resistance of the riveted stringer-to-cross-girder connection in terms of the use of European standards. The results of fatigue tests performed on specially prepared test samples are presented with the aim to define the fatigue detail category.

Keywords: riveted bridges; stringer-to-cross-girder connection; bending stiffness; hinged connection; rigid connection; fatigue tests; fatigue detail category

Citation: Gocál, J.; Vičan, J.; Jošt, J. Real Stiffness and Fatigue Resistance of Stringer-to-Cross-Girder Connection of Riveted Steel Railway Bridges. *Appl. Sci.* **2023**, *13*, 2278. https://doi.org/10.3390/app13042278

Academic Editors: Tong Guo and Zhongxiang Liu

Received: 5 January 2023
Revised: 6 February 2023
Accepted: 8 February 2023
Published: 10 February 2023

1. Introduction

Steel riveted bridges built after the Second World War or even earlier still represent, in terms of number, a significant type of bridge superstructure on railway lines in Slovakia but also in Europe. During their service life, they have often been exposed, in addition to adverse environmental effects, to the escalating effects of traffic loads that have significantly exceeded those for which they were originally designed [1–6], both in terms of the values of the axle forces and the total volume of traffic. As a result, these structures are very often subject to the increased effects of fatigue degradation processes. The origin and development of fatigue cracks on old steel riveted bridges are also related to commonly used structural details at the time of their design as well as to the insufficient description of their actual behaviour in global analysis using more or less simplified computational models of the bridge superstructures. Naturally, degradation caused by corrosion processes also contributes to the increased occurrence of fatigue damages, especially in the case of neglected maintenance of steel bridges [7,8], resulting both in the creation of notched details prone to fatigue cracking and in increased stress of critical cross sections weakened by corrosion losses [9–12].

Steel girder bridges with open member decks belong to the most frequently used types of superstructures of old riveted steel railway bridges. Depending on the length

and nature of the bridged obstacle, the main girders may be designed as plate girders, truss girders or as bowstring girders (so-called tied-arch bridges). The member bridge deck consists of cross girders and longitudinal beams (stringers) on which the rails are attached by means of usually wooden sleepers. Depending on the position of the bridge deck in relation to the main girders, we then distinguish between bridges with an upper deck (so-called deck bridges), bridges with a lower deck (called through bridges) or bridges with an intermediate bridge deck (half-through bridges).

Regardless of the type of main girders or the position of the bridge deck, the bridge deck members are usually the ones that are most affected by the aforementioned negative factors. A usually greater extent of corrosion attack of these members is related to a greater accumulation of moisture under the sleepers or more humid air under the sheets covering the sleepers and the bridge deck members themselves but also with potentially unwanted leaks of aggressive chemical substances from rail vehicles passing over the bridge. The more frequent occurrence of fatigue damage, in turn, is related to the direct dynamic stressing of bridge deck members caused by the passage of trains resulting in a significantly greater number of load cycles.

One of the typical cases of fatigue damage on steel riveted bridges is a fatigue crack in the web of the stringer at the point of its connection to the cross girder (Figure 1), which is realised only by connecting the webs of the stringer and the cross girder to each other using connecting angles while the flanges of the adjacent stringers are not connected. At the time of the design of the mentioned types of bridges, such a connection was commonly considered to transmit only axial force and shear force in the plane of the web. Based on this simplifying assumption, no fatigue crack was expected to develop in this detail during the bridge service life. However, the relatively frequent occurrence of fatigue cracks indicates the incorrectness of this assumption. To explain this phenomenon, it is possible to consider that, although not great, a certain real bending stiffness of this connection has resulted in higher normal stresses in the web of the stringer at the upper edge, mainly tensile, due to hogging moment. Increased concentration of normal stresses usually in the place of the first rivet connecting the web plate and the flange angles, in combination with a large number of loading cycles, have led to the initiation and subsequent growth of a fatigue crack. The bending stiffness as well as the fatigue resistance of the stringer-to-cross-girder connection is the subject of several works, e.g., [13,14]. However, they are focused on fatigue cracks in the connecting angles as well as rivet failures, not on cracks in the stringer web as shown in Figure 1.

Figure 1. Illustrative picture of a fatigue crack occurrence in the web of the stringer.

The configuration of the stringer-to-cross-girder connection underwent a certain development, especially during the second half of the last century, together with the development of welded structures using preloaded bolted joints, with the aim of achieving a smoother flow of stresses in the stringers at the connection point. In the first part, this article focuses

on an analysis of the bending stiffness of the aforementioned structural detail with different structural arrangements. Subsequently, attention is paid to fatigue resistance of a riveted stringer-to-cross-girder connection in terms of the use of European standards.

2. Stiffness of the Stringer-to-Cross-Girder Connection

The bending stiffness of the stringer-to-cross-girder connection depends primarily on the way in which the flanges of two adjacent stringers are interconnected. In the case of old riveted bridges, the connection of stringers was usually solved only by connecting the webs of the stringers using connecting angles, while the flanges were not connected at all (Figure 2a). Therefore, in global analysis, such a connection was considered by default as a hinged one, i.e., transmitting only shear and normal forces. In the case of a structural modification with a strengthening haunch according to Figure 2b, primarily aimed at increasing the shear resistance of the connection and also reducing the span of the stringer, a certain small increase in bending resistance can also be assumed.

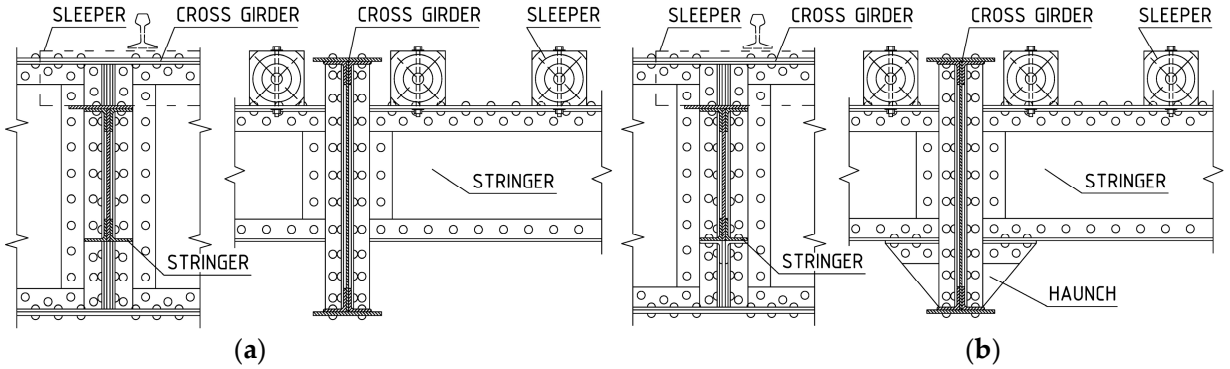

Figure 2. Arrangement of a typical stringer-to-cross-girder riveted connection (**a**) without a reinforcing haunch and (**b**) with a reinforcing haunch.

A significant increase in bending stiffness and resistance of this connection was achieved in the 1970s with the expansion of welded structures and bolted joints by supplementing the previous structural modification (Figure 2b) with the connection of the upper flanges of the adjacent stringers with a splice plate passing through a slot cut in the web of the cross beam (Figure 3a). Although the lower flanges are not connected to each other, the compressive stresses in their level from the negative bending moment are transferred by direct contact, so this detail can be considered partially continuous. The complete continuity of the stringers was achieved only by the structural arrangement according to (Figure 3b), in which, in addition to the webs, both flanges of the longitudinal members are also interconnected using splice plates.

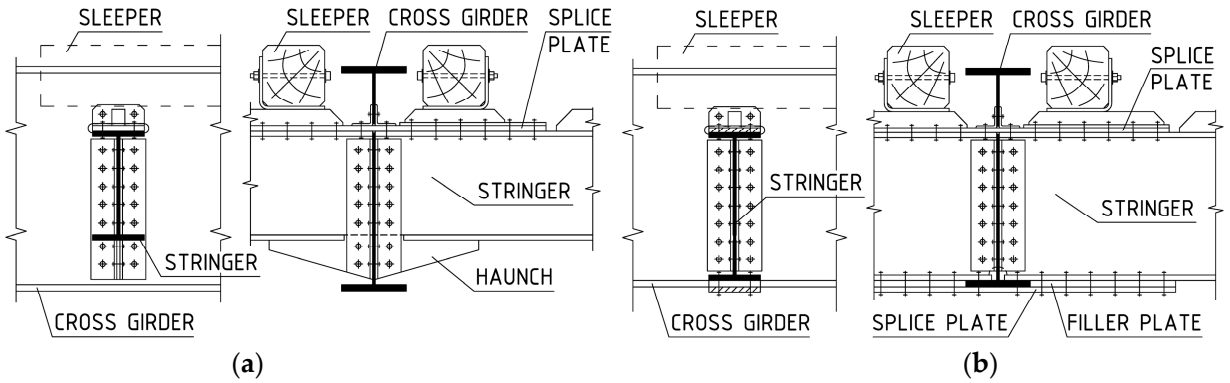

Figure 3. Arrangement of a typical stringer-to-cross-girder bolted splice connection (**a**) without lower flange connection and (**b**) with both flanges connection.

2.1. Theoretical Study

The analysis of the bending stiffness of the stringer-to-cross-girder connection was the subject of a parametric study, which we have processed in our department. In this study, we observed the influence of different configurations of a stringer-to-cross-girder connection corresponding to those in Figures 2 and 3 on the bending moment in the stringer at the place of its connection to the cross girder. Three types of joint configurations were considered in this study:

- Type 1—stringers are connected to the cross girder by their webs only using connecting angles;
- Type 2—in addition to the web connection, the upper flanges of the adjacent stringers are also interconnected using splice plates. The lower flanges are not connected directly, but the bottom part of the joint is stiffened by haunches;
- Type 3—in addition to the web connection, both stringer flanges are interconnected using splice plates.

Theoretical analysis of the behaviour of these three types of connections was carried out using three different types of finite element models (FEM models) of a fictitious superstructure of a plate girder bridge with a lower member deck. The numerical models were processed with SCIA Engineer software [15]. The two models represented a common way of modelling this type of bridge when all the structural members of the superstructure were modelled with beam elements (Figure 4a,c). The stringer-to-cross-girder connection was considered once as fully hinged and once as a perfectly rigid joint. In the third model, the whole superstructure was modelled using shell elements for all load-carrying structural members (Figure 4b). Such a model allowed for a better approximation of the behaviour of the analysed type of connection at the cost of a more demanding modelling process as well as the necessary computing time.

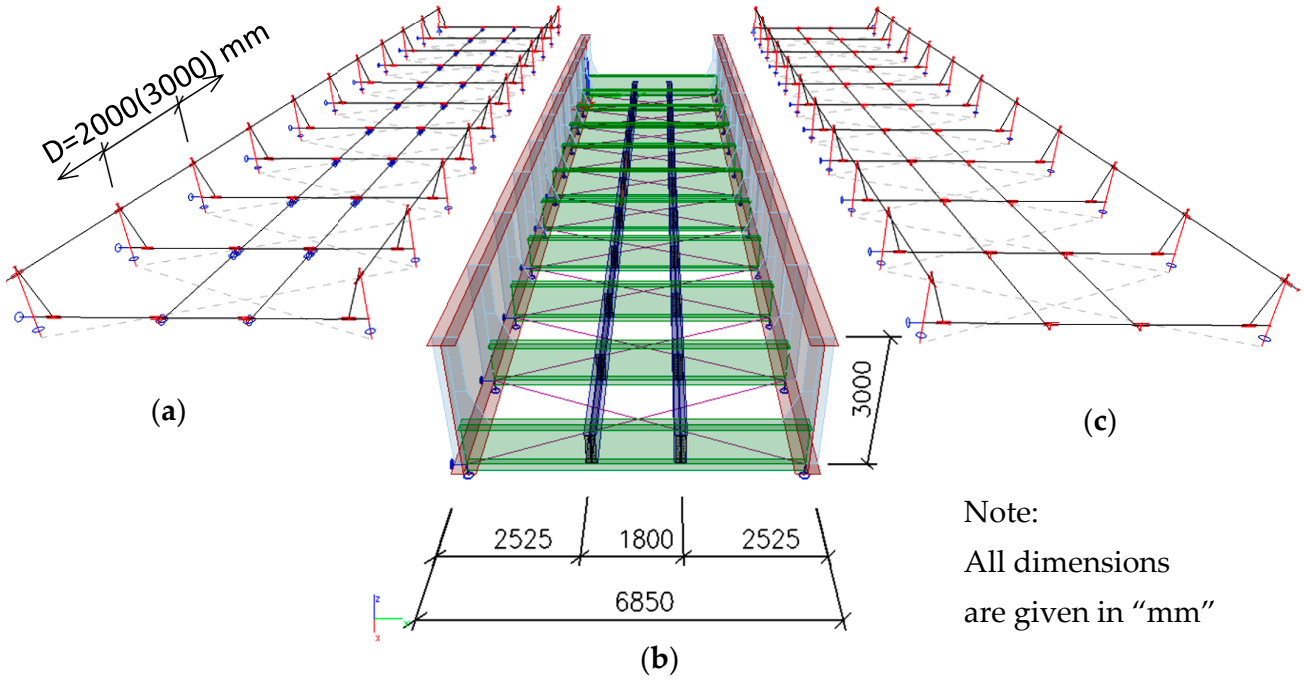

Figure 4. Three types of numerical models of the bridge superstructure: (**a**) beam FEM model with hinged stringers, (**b**) shell FEM model, (**c**) beam FEM model with continuous stringers.

Visualizations of the shell models of the three considered types of stringer-to-cross-girder connections are illustrated in Figure 5. The bolts joining the connecting angles and webs of the stringers and cross girders as well as the splice plates and stringer flanges were modelled by means of beam elements rigidly connected with the shell elements

modelling webs, flanges and angles. The shell elements modelling the cross girders were rigidly connected to the shell elements modelling the main girders including vertical stiffeners. Standard rectangular 2D finite elements were used in the mesh generation by the computational program. The average size of the 2D elements was considered to be 150 mm, with a refinement to the value of 20 mm in the case of the examined stringers and 10 mm in the case of the connecting angles. Two different spans of stringers, given by the cross girder distances D, have been considered for each investigated case in this study, namely D = 2.0 m and D = 3.0 m. Thus, 18 numerical models were processed for the needs of this study in total. In order to eliminate the global effects of the considered loads, the main girders were supported in the vertical direction at the locations of the cross-girder connections.

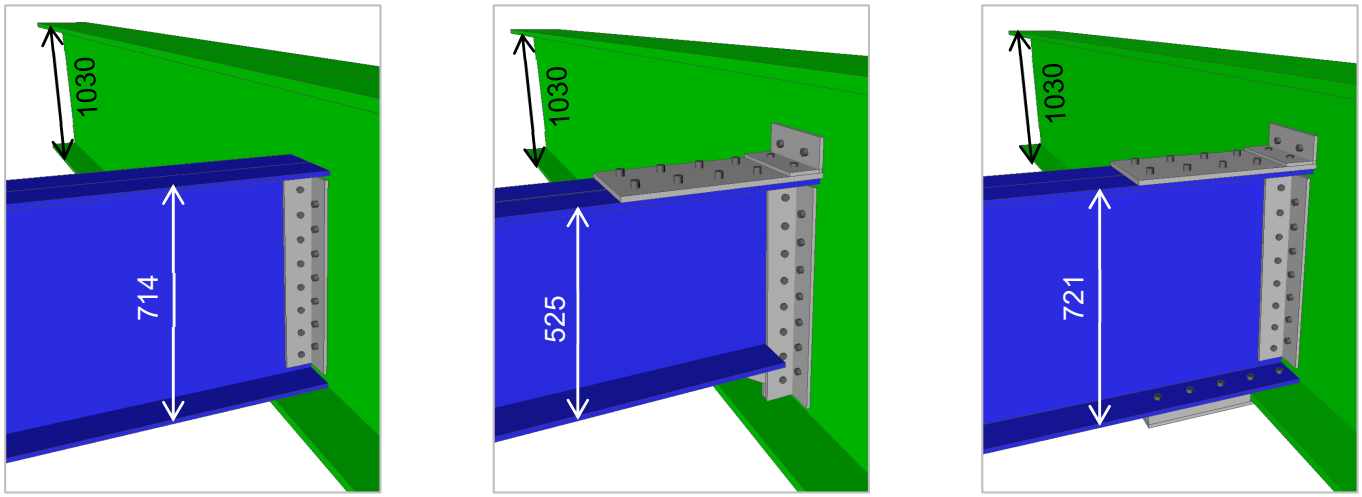

(**a**) (**b**) (**c**)

Figure 5. Shell FEM model visualisations of the different connection types: (**a**) Type 1; (**b**) Type 2; (**c**) Type 3.

The results of the theoretical study are presented in Figure 6. The bending stiffness of the observed three types of stringer-to-cross-girder connections is compared indirectly by means of the courses of bending moments from the uniformly distributed load on an intermediate stringer calculated with respect to the different boundary conditions as they are presented hereinbefore. The bending moments are given in a relative scale related to the minimum calculated moment corresponding to the beam FEM model with a perfectly rigid stringer-to-cross-girder connection ($M_{y,min,RC}$). The results of the numerical analysis confirmed the expected behaviour of the three investigated types of stringer-to-cross-girder connections. The behaviour of the Type 1 connection is close to perfectly hinged, although from the moment diagrams in Figure 6, a certain stiffness of this connection is evident when the bending moment above the cross girder reaches about 19% of the bending moment on the perfectly rigidly connected stringer with a span of D = 3.0 m, or about 14% in the case of the stringer with a span of D = 2.0 m. On the contrary, the behaviour of the Type 3 connection is very close to perfectly rigid when the bending moment above the cross girder reaches 87% or 86% of the one on the perfectly rigidly connected stringer with a span of D = 3.0 m or D = 2.0 m, respectively.

It is obvious that for common practical modelling using beam FEM models, the Type 1 connection can be modelled with sufficient accuracy as fully hinged, while the Type 3 connection can be modelled as fully rigid. However, if it is necessary to analyse the stresses in the joint area in more detail, it may be necessary to model the Type 1 connection more accurately. Alternatively, the effect of the partial stiffness of the Type 1 connection can be taken into account simply by considering a local hogging moment above the cross girder equal to 15% of the bending moment in the middle of the hinged stringer. The behaviour

of the Type 2 connection is somewhere between Type 1 and Type 3 when the bending moment above the cross girder reaches 62% or 52% of the bending moment on a perfectly rigidly connected stringer with a span of D = 3.0 m or D = 2.0 m, respectively. Although it nears more to the rigid behaviour, especially in the case of the longer stringer span of D = 3.0 m, this type of connection requires a generally more precise way of modelling, e.g., as a semirigid connection. As a simplification for practical use, assuming the application of a rigid model of the Type 2 connection, it is possible to take into account its real stiffness by reducing the local hogging moment above the cross girder by 20% and, at the same time, increasing the local sagging moment in the middle of the stringer by 80%. Alternatively, when assessing the splice plates connecting the upper flanges of the stringers, it is possible to determine the normal force in it by dividing the bending moment determined for the case of a rigid connection by the distance between the centres of gravity of the stringer flanges, increased by one-third of the end haunch height.

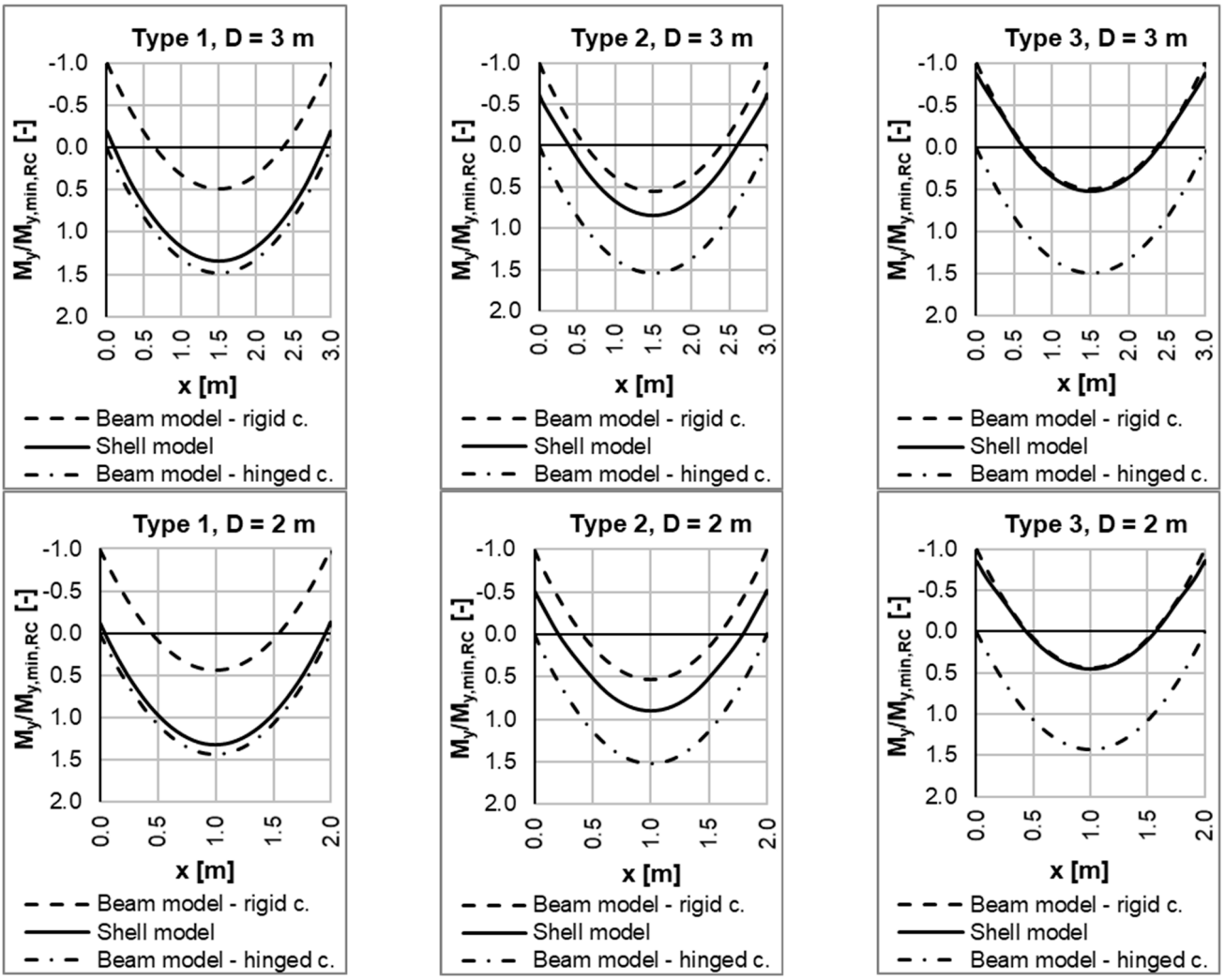

Figure 6. Relative bending moment diagrams M_y of the stringers with different span D and types of connections to the cross girder.

2.2. Experimental and Numerical Analyses of a Real Railway Bridge

In order to verify the validity of the results of the presented theoretical study, also in the case of riveted bridge structures, we performed another experimental–numerical analysis on a real steel riveted bridge. The observed bridge is situated near the railway station in Turany at km 303.309 of the Žilina–Košice track. The investigated superstructure

forms the first span of a three-simple-span truss bridge with a lower member deck. The theoretical span of the main girders is 43.4 m.

The bridge superstructure with a width of 5.510 m consists of two main truss girders with a theoretical height of 4.500 m. The length of one field of the truss structure is 4.340 m. The open member bridge deck is created with stringers with a length of 4.340 m and cross girders. The global depth of the riveted plate-girder stringer is 600 mm, and it is created with a web made of P 14 × 586 mm and flanges made of angles L 100 × 100 × 14 mm. The riveted cross girder of 1130 mm high is created with a web made of P 14 × 1100 mm, flanges made of angles L 140 × 140 × 14 mm and a sheet P 15 × 320 mm.

The bridge was built in 1950 from steel 10,372 (according to previous Czechoslovak standard ČSN 1230) corresponding to the current designation of the steel strength class S235. At the time of testing, the bridge was in very good condition.

The bridge superstructure was analysed using a beam FEM model by means of SCIA Engineer software [15]. The members of the main truss girders are connected rigidly, while the connections of the cross girders and the horizontal bottom bracing members to the main girders are considered fully hinged. The superstructure was, similarly to the theoretical study, analysed using two types of numerical models, one with hinged stringers and one with rigidly connected stringers. The numerical analysis with a shell FEM model was replaced by an experimental analysis using strain gauges, with the help of which we recorded the stress response of the structure to a real railway traffic load on the chosen stringer in the stringer midspan and near its connection to the cross girder. The measured records of the stress response in the monitored locations were subsequently confronted with the records obtained using numeric simulations of train sets by means of FEM models. During the experimental measurements, the passage of 23 train sets was recorded, namely, 7 freight trains, 8 express trains and 8 passenger trains. The necessary technical data on the train sets (the type of locomotive, the type and number of wagons and the corresponding values of axle forces and their distances) were obtained from the operational information system, which is disposed of by the railway operator of the Slovak Republic.

A view of the bridge and scheme of the numerical model of the superstructure are presented in Figures 7 and 8, respectively. The basic geometric parameters of the bridge cross-section are evident in Figure 9. The second stringer from the support was chosen for the analysis. Its connection to the cross girder is made similarly to Type 1 in the theoretical study (Figure 5), i.e., by connecting only the webs using connecting angles but with the use of stiffening haunches. The geometric parameters of the connection as well as the placement of strain gauges installed on the chosen stringer are presented in Figure 10.

A comparison of the stress responses in the selected locations obtained from the experimental measurements as well as from the numerical simulations using the beam FEM model in Figure 8 is illustrated in the graphs in Figure 11, where the time courses of the stress response to the passing train set consisting of one electric locomotive of the 162 series and eight-passenger wagons are presented. The locomotive and each of the passenger wagons was characterised by axle forces 4 × 212.5 kN and 4 × 112.5 kN, respectively. In order to eliminate the horizontal effects of the real railway traffic load, the average values of the corresponding pairs of normal stresses recorded in the monitored locations of the bottom and top flange of the stringer were evaluated, i.e., (S0, S1) and (S2, S3) in the bottom and the top flange, respectively, in the middle of the stringer as well as (S4, S5) and (S6, S7) in the bottom and top flange, respectively, near the cross girder.

It can be seen that the stiffness of the stringer-to-cross-girder connection in Figure 10 is significantly influenced due to strengthening haunches connecting the stringer bottom flange with the cross-girder bottom flange. This connection considerably increases the joint stiffness so that its behaviour seems to be closer to the rigid one than to the nominally hinged connection. At the same time, however, it should be noted that the stress response courses also include, in addition to the local effects of the traffic load on the stringers, global effects due to the cooperation of the bridge deck with the main girders. In this case, the local and global effects cannot be separated as in the theoretical study where

we separated the local effects by simply supporting the main girders at the cross-girder connection points. The total stress consisting of local, mainly bending, stresses and global, mainly axial (tensile), stresses due to the cooperation is thus influenced not only by the bending stiffness of the connection but also by its normal stiffness. In addition, the degree of cooperation of the bridge deck with the main girders is also partially influenced by the bending stiffness of the connection of the cross girders to the main girders in the horizontal direction, which was considered as nominally hinged in the numerical analyses (Figure 8). Considering the certain stiffness of this joint, the stresses in the stringer would be affected due to the higher cooperation of the bridge deck with the main girders. Therefore, in order to minimize these effects, a stringer near the abutment, where the interaction effects are not very significant, was chosen for the analysis.

Figure 7. View of the bridge in Turany.

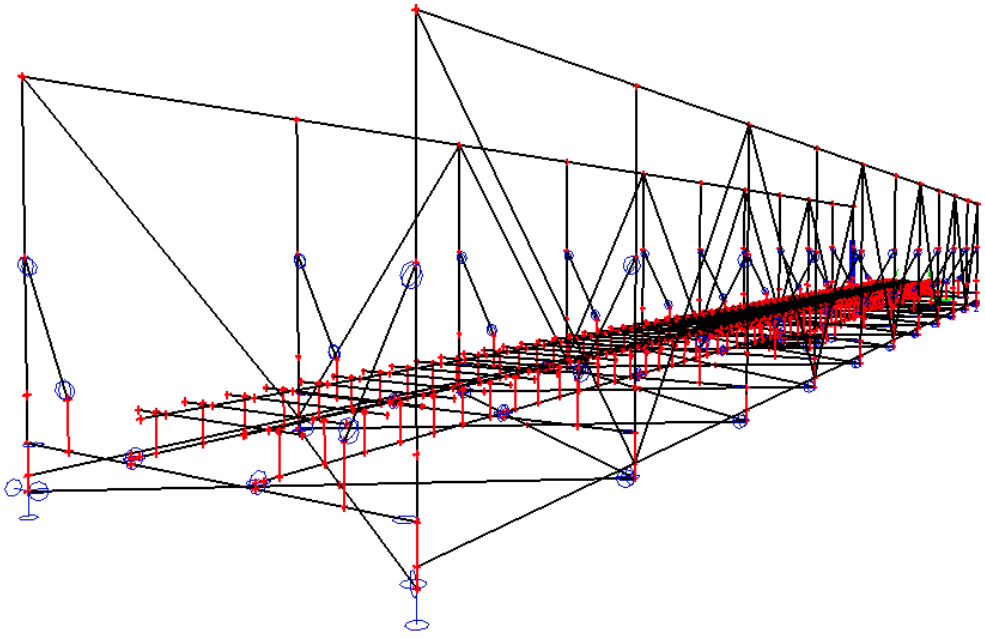

Figure 8. Numerical beam FEM model of the bridge superstructure.

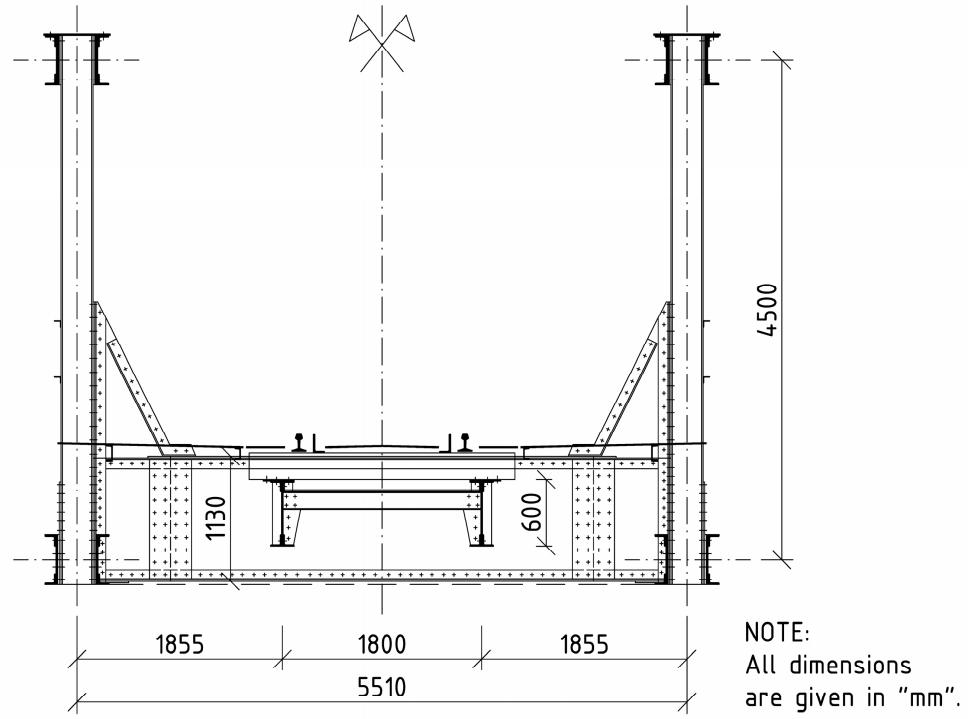

Figure 9. Cross-section of the bridge superstructure in Turany.

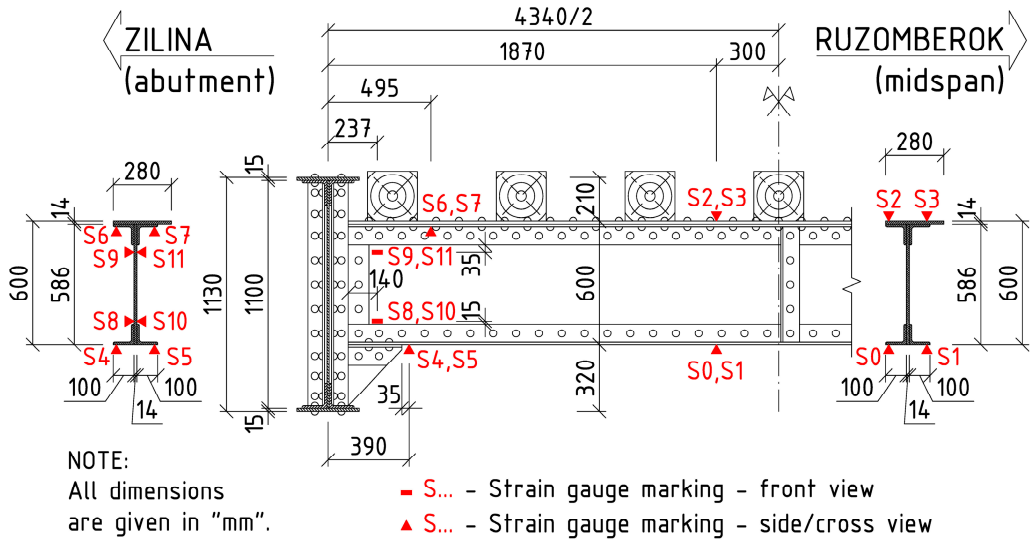

Figure 10. Configuration of the chosen stringer-to-cross-girder connection and placement of strain gauges.

2.3. Discussion of the Theoretical and Experimental Analyses Results

The results of the theoretical analyses confirmed the fundamental importance of the connection of the flanges of the two adjacent stringers connected to the cross girder in terms of the rigid behaviour of the joint. The joint including the connection of both the upper and lower flange (Type 3 in Figure 5) ensures the full continuity of the stringers, and thus its modelling with a rigid connection reliably describes its real behaviour. The joint without mutually connecting the lower flanges of the stringers (Type 2 in Figure 5) shows a semirigid behaviour and generally requires more accurate modelling. In common practical cases, it is possible to use a perfectly rigid connection with the consideration of certain local bending moment corrections. The Type 1 connection realised only by connecting the webs of the stringers and cross girders using connecting angles can be modelled in common cases

as nominally hinged. However, in order to better consider the stresses near the connection, even in this case, it is necessary to take into account the partial stiffness of the connection in a more appropriate way.

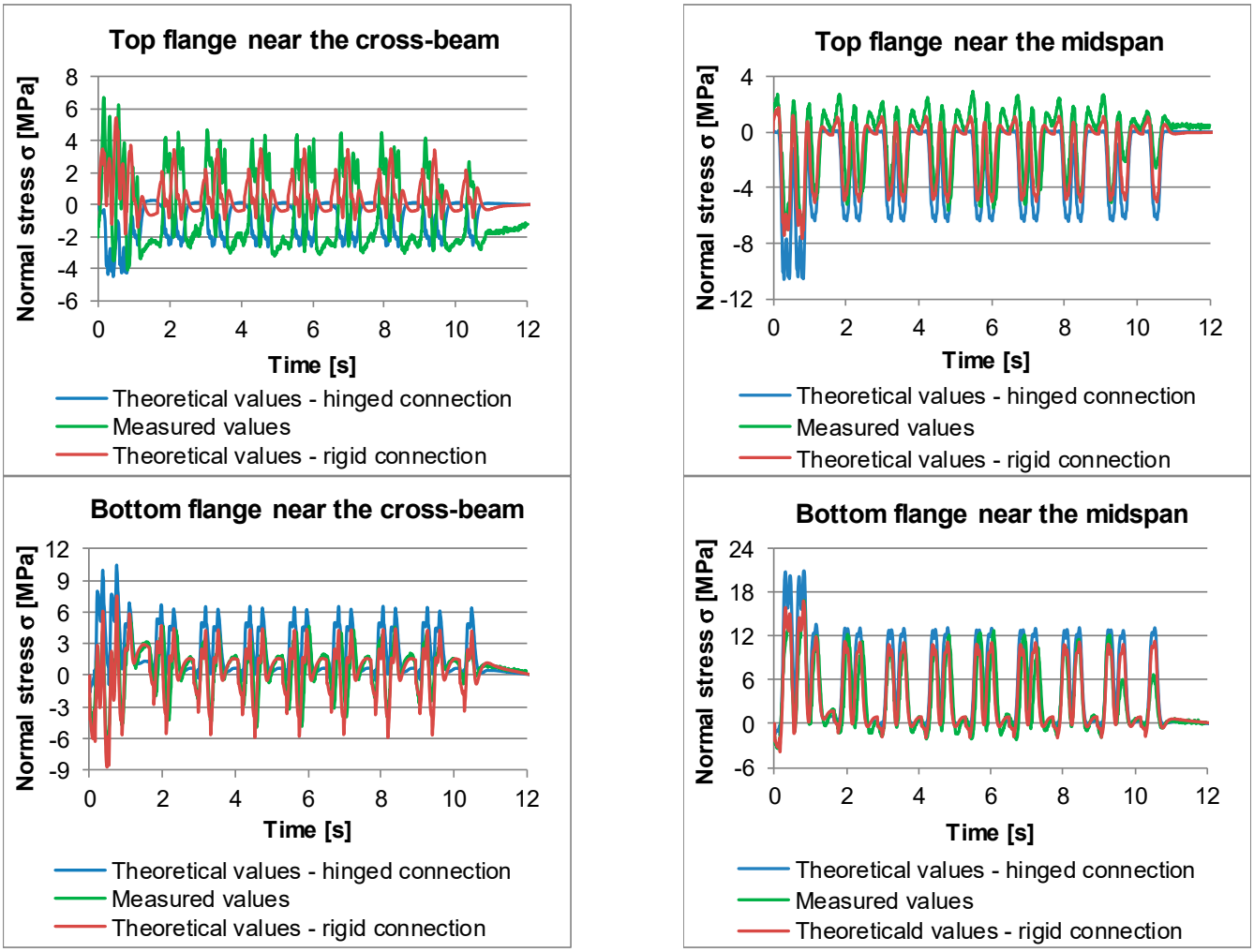

Figure 11. Courses of the stress response in the chosen locations of the stringer.

Experimental and numerical analyses on the real riveted bridge structure in principle confirmed the validity of the conclusions from the theoretical analyses. The influence of the strengthening haunches under the lower flange of the stringers has been shown to be important. In addition to the shear resistance of the connection, the haunch also significantly increases its bending stiffness, even in the case of the unconnected upper flanges of the stringers. At the same time, the experimental analysis pointed out the more complicated stress state near the riveted connection, which cannot be adequately described using simple computational models of the connection.

3. Fatigue Resistance of the Riveted Stringer-to-Cross-Girder Connection

The fatigue assessment of dynamically loaded structures according to standard methods is generally based on evaluating critical structural details prone to fatigue failure, which are classified into corresponding standard fatigue categories. After assigning a detailed category, the structural detail can be assessed using the appropriate S-N curve, which relates the design fatigue life of the detail to the constant cyclic stress range caused by the variable load. Since the greatest research expansion in the field of fatigue resistance of steel structures and bridges is connected with the development of steel welded structures in the second half of the last century [16,17], this fact has subsequently been reflected in the

European standard methodology for assessing the fatigue resistance of steel structures. Knowledge regarding the ability of riveted structures to withstand the fatigue process had not initially been investigated to the same extent as for modern welded structures. Therefore, Eurocode 3 [18] does not give relevant instructions for assessing the riveted details. More extensive research in the field of the fatigue of riveted structures began to take place at the turn of the 20th and 21st centuries. Currently, quite a lot of works dealing with this issue are already available [19–29], in which some recommendations for the categorisation of typical riveted structural details prone to fatigue failure can be found. In our department, we have focused on the fatigue behaviour of the aforementioned structural detail, i.e., the stringer-to-cross-girder connection, which is typical for the occurrence of fatigue cracks. We have performed the laboratory fatigue tests of this detail to define its fatigue detail category according to Eurocode 3 [18].

3.1. Laboratory Specimens

Due to the effective use of the limited possibilities of the used hydraulic pulsator as well as for economic reasons, we chose a cantilever beam loaded with a force at the free end as a static scheme when designing the test samples (Figure 12). The use of a standard simply supported stringer would require the use of up to eight times the pulsating loading force or eight times the length of the test specimen or some suitable combination. Initially, six test samples were made of steel S235 with the following guaranteed yield and ultimate strength characteristics: f_y = 235 MPa, f_u = 360 MPa. The I-cross-section of the stringer samples consisted of the web from steel plate P 10 × 390 mm and flanges from two angles L 80 × 80 × 8 mm. The flange angles were connected to the web by means of 22 mm diameter rivets. The stringer was connected to the cross girder of hot-rolled profile IPE 700 by means of two connecting angles L 80 × 80 × 8 mm and 16 high strength bolts M24-8.8. Three of the samples denoted as Type A were made without stiffening haunches, and three (Type B) were reinforced with triangular haunches at the connection point.

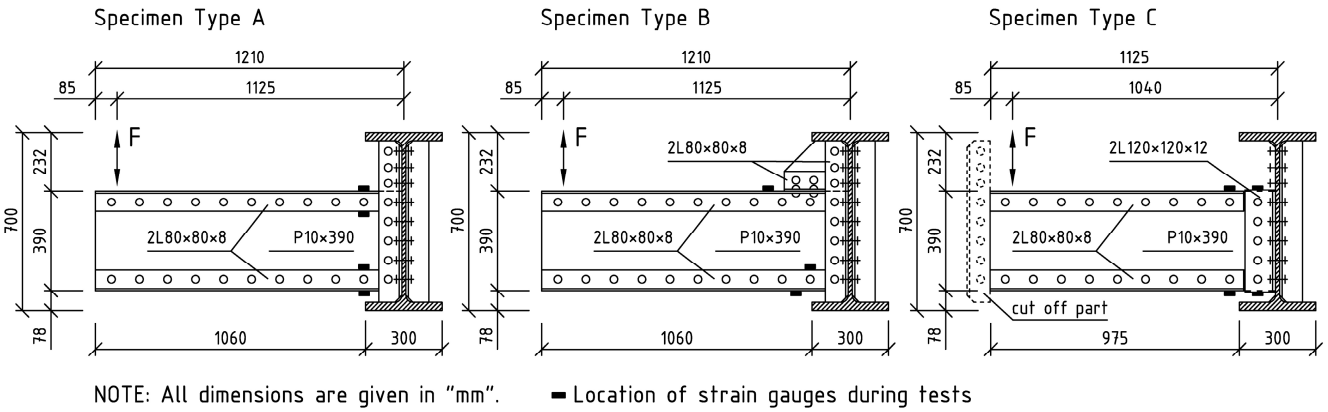

Figure 12. Configuration of laboratory specimens and arrangement of strain gauges.

After these six samples were tested, another five test specimens without reinforcing haunches were prepared by modifying them, designated as Type C. One of the original six samples was used for necessary material destructive tests. The new connecting angles 2 L 120 × 120 × 12 mm were shortened in order to situate strain gauges above the first and below the last rivet, respectively. A total of eleven test samples were thus tested.

3.2. Fatigue Tests

The parameters of the fatigue tests, related mainly to the values of the amplitudes of the acting variable forces, were determined using numerical shell FEM models in the SCIA Engineer software (Figure 13), which were subsequently calibrated according to the test results and used for further numerical analyses. Standard rectangular 2D finite elements were used in the mesh generation by the computational program. The average size of the

2D elements was considered to be 20 mm, with a refinement to the value of 10 mm in the case of the web of the stringer as well as the connecting angles. The considered material characteristics corresponded to the material of the tested samples, i.e., steel class S235. The linear stress–strain diagram was used in the models.

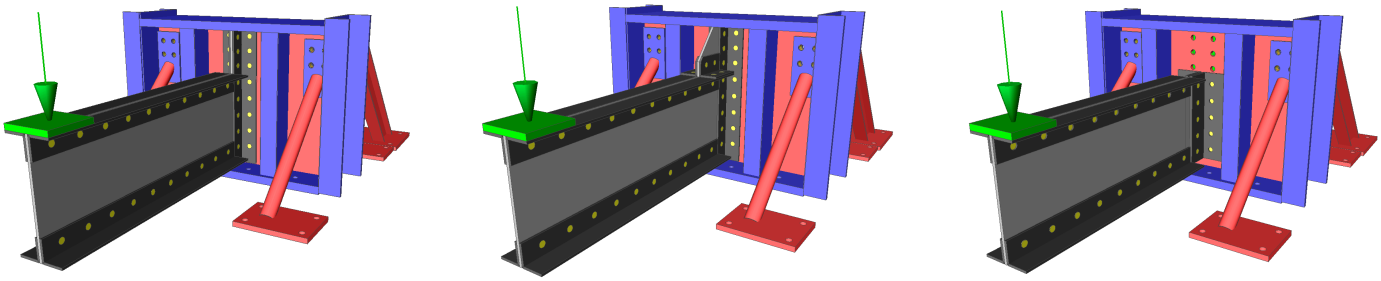

Figure 13. Visualisation of numerical shell FEM models of the test samples.

All test specimens were tested under a variable moment load induced by an alternating force acting on the free end of the cantilever with constant amplitude. The upper and lower limits of the alternating force were gradually chosen for individual samples in such a way as to induce alternating stress with different levels of the stress range at the critical section, i.e., so that the normal stresses oscillate around a zero value. The range of the loading force, and thus also the induced normal stress, were constant during the entire fatigue test of the individual sample. Normal stresses in the stringer web were noticed by means of strain gauges located according to Figure 12. Illustration photos from the fatigue tests are presented in Figure 14.

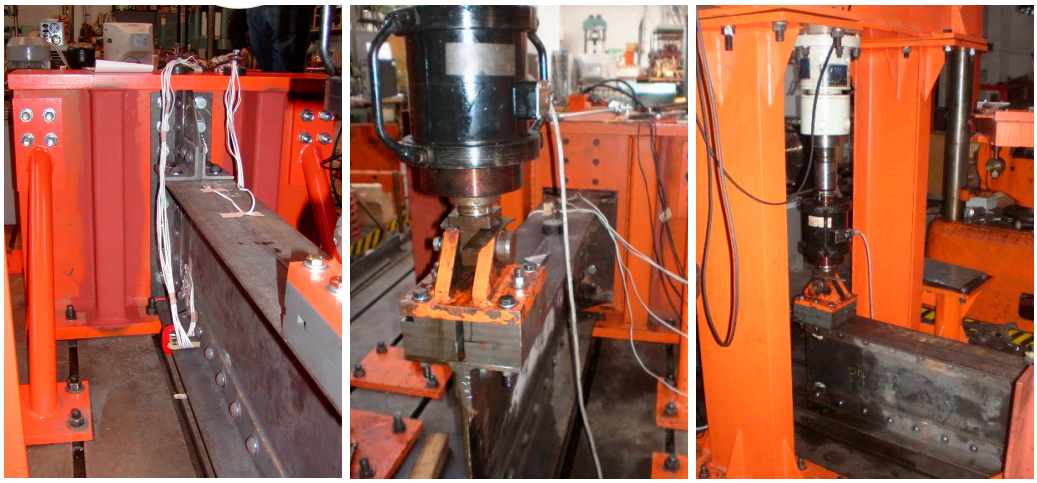

Figure 14. Illustration photos from fatigue tests.

3.3. Fatigue Test Results

The crack initiation was considered the failure criterion during the tests. Since the rivet holes were covered by the connecting angles, the initiation of the fatigue crack was difficult to follow. However, extensive plasticization around the rivet holes and subsequent crack initiation caused significant deformations of the free end of the monitored sample where the alternating force was acting. Then, it was a problem to ensure the set vibration mode of the sample, and the test had to be stopped. Thus, fatigue failure was defined indirectly as the inability of the specimen to sustain the applied load. Typical failures of the investigated detail are presented in Figure 15. The failures themselves were recorded only after the samples were disassembled when the tests were completed. The picture on the left side shows the out-of-roundness of the hole diameter due to material cyclic plasticity, after which, the global deflection of the beam increased rapidly. The right figure shows the

final failure of one sample induced by static loading only after finishing the fatigue test itself. Although a total of eleven fatigue tests were performed, we could finally use the results of only ten to determine the fatigue detail category, as in one case, the fatigue crack did not appear in the web of the stringer (Figure 15) but in the connecting angle (Figure 16). The shape of the growing fatigue crack is somewhat different from the shape that appears on real stringers (Figure 1). The difference is due to the different static scheme of the test specimens, which was chosen as a cantilever beam for both practical and economic reasons. The actual stringer with the connection to the cross girder according to Figure 1 can be considered at the beginning of its service life as a beam with a semirigid connection to the cross girder on both sides, albeit with relatively low bending stiffness. In the case of the fatigue crack origin, the bending stiffness of the cross-section at the connection point gradually decreased with the gradual crack growth, which made the static scheme of the stringer closer and closer to a double-hinged beam. The result is a gradual decrease in the bending moment in the connection and the related redistribution of stresses in the stringer. It is reflected by the gradual curvature of the shape of the crack growing in the direction perpendicular to the main tensile stresses, as well as by slowing down or even stopping the crack growth. On the other hand, in the case of the cantilever, which is a statically determinate structure regardless of the actual stiffness of the joint (higher than zero, of course), the bending moment at a constant loading force is constant even in the case of fatigue crack development, and the direction of the main tensile stresses does not change much. However, this discrepancy in the static schemes does not have a fundamental impact on the recorded design life of the investigated detail because the design life (in terms of fatigue) is generally related to the crack initiation, and it is reasonable to assume that the crack initiation period will be the same for both static schemes.

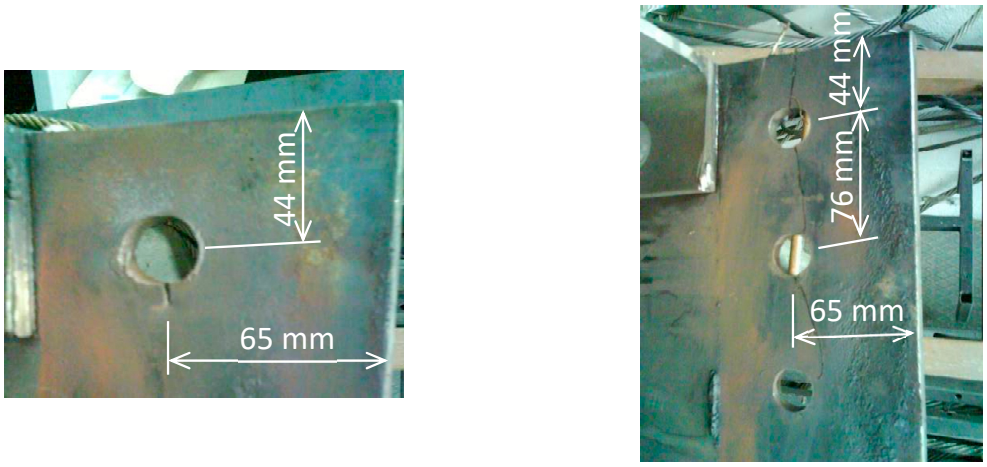

Figure 15. Fatigue cracks in the web of stringer.

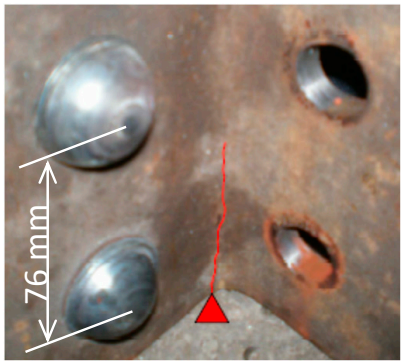

Figure 16. Fatigue crack in the connecting angle.

The results of fatigue tests in the form of normal stress ranges and the corresponding numbers of load cycles to the fatigue failure are summarized in Table 1. The stress range values determined from the measurements during the experiments had to be modified, as the mean stress value was always a little different from zero, but the standard S-N curves of fatigue resistance are derived for fully reversed loading. The nonzero value of the mean stress was caused on the one hand by the structural asymmetry of the joint (Specimen Type B) and, on the other hand, by the asymmetric behaviour of the preloaded bolted joint subjected to a perpendicular bending moment, where only the cross-sectional area of the screws acted in the tensioned part of the joint, while the entire contact compression area of the angle flanges adjacent to the cross-girder web was effective in the compressed part. To modify the stress ranges with nonzero mean stress, we used the Goodman relation [30]:

$$\frac{\sigma_a}{\sigma_e} + \frac{\sigma_m}{f_u} = 1, \tag{1}$$

where σ_a is the alternating stress amplitude with nonzero mean stress $\sigma_m \neq 0$, σ_e is the fully reversing stress amplitude corresponding to the mean stress $\sigma_m = 0$ and f_u is the ultimate strength of the material. From Equation (1), the fully reversing stress amplitude σ_e can be derived as follows:

$$\sigma_e = \frac{\sigma_a}{1 - \frac{\sigma_m}{f_u}}, \tag{2}$$

Table 1. Results of fatigue tests.

Specimen No.	Specimen Type	Equivalent Stress Range $\Delta\sigma_e$ [MPa]	Number of Cycles to Failure N [cycles]
1	A	97.2	2,218,900
2	A	147.7	629,000
3	A	125.4	798,350
4	B	114.9	1,276,750
5	B	136.6	571,000
6	B	88.0	3,653,000
7	C	121.7	1,240,450
8	C	116.3	1,863,760
9	C	142.5	1,406,080
10	C	119.0	1,697,600

3.4. Determination of the Fatigue Detail Category

For high-cycle fatigue of steel structures, the relation between the applied stress range $\Delta\sigma$ (also denoted as S) and the corresponding number of stress cycles N to fatigue failure follows an exponential law given by the well-known equation

$$N = C \cdot \Delta\sigma^{-m}, \tag{3}$$

which is, for practical reasons, usually indicated in logarithmic form.

$$\log N = \log C - m \cdot \log \Delta\sigma, \tag{4}$$

where m is a parameter indicating the slope of the S-N curve in logarithmic form (4) and C (or log C) is a parameter dependent on the type of notch detail representing the intercept of the S-N curve on the horizontal axis, i.e., the theoretical number of cycles corresponding to the stress range $\Delta\sigma = 1$ MPa, or $\log \Delta\sigma = 0$.

Based on the experimental data in the form of n coordinate pairs $[\Delta\sigma_i, N_i]$, the parameters C and m can be calculated using the procedures of mathematical statistics [31], namely, linear regression analysis.

According to the procedure in origin, Slovak standard STN 73 1401 [32], the parameter $\log \Delta\sigma$ represents an independent variable ($x_i = \log \Delta\sigma_i$), and log N represents a dependent

variable ($y_i = \log N_i$) with a normal probability distribution. Then, the regression line for 50% survival probability can be expressed by the equation

$$y = \alpha + \beta \cdot x, \tag{5}$$

in which the parameters α and β corresponding to the parameters log C and m, respectively, in Equation (4) and can be calculated as follows:

$$\beta = \frac{\sum x_i y_i - \frac{1}{n}(\sum x_i)(\sum y_i)}{\sum x_i^2 - \frac{1}{n}(\sum x_i)^2};\ \alpha = \frac{\sum y_i - \beta \sum x_i}{n}, \tag{6}$$

The stress range $\Delta\sigma_P$ on the regression line corresponding to the number of cycles $N = 2 \times 10^6$ is

$$\Delta\sigma_P = \left(\frac{2 \times 10^6}{10^{\alpha}}\right)^{1/\beta}. \tag{7}$$

The left-sided prediction limit of $\log N_P$ corresponding to the stress range $\Delta\sigma_P$ is given by the formula

$$\log N_P = \log\left(2 \times 10^6\right) - t_{0.05,n-2} \cdot s_R \cdot \sqrt{1 + \frac{1}{n} + \frac{(\log \Delta\sigma_P - (\sum x_i)/n)^2}{\sum x_i^2 - \frac{1}{n}(\sum x_i)^2}}, \tag{8}$$

where $t_{0.05,n-2}$ is the fifth percentile of the Student's t-distribution with n–2 degrees of freedom (it means 95% survival probability), and s_R is the standard deviation given by the formula

$$s_R = \sqrt{\frac{1}{n-2}\left(\sum y_i^2 - \frac{1}{n}(\sum y_i)^2 - \beta \cdot \left(\sum x_i y_i - \frac{1}{n}(\sum x_i)(\sum y_i)\right)\right)}. \tag{9}$$

Finally, the characteristic stress range for the determination of the detail category can be calculated from the equation

$$\Delta\sigma_C = \Delta\sigma_P \cdot \left(\frac{2 \times 10^6}{N_P}\right)^{1/\beta}. \tag{10}$$

Applying the procedure mentioned above and using the data in Table 1, we have determined the values of parameters $\alpha = 12.41$, $\beta = -3.02$ and the characteristic value of stress range $\Delta\sigma_C = 83.9$ MPa.

General principles for statistical evaluation of experimental tests according to Eurocode are given in EN 1990, Annex D [33]. A more detailed procedure for evaluating fatigue tests can be found in the background document [34] to EN 1993-1-9 [15]. Application of these procedures can be found in works [35,36]. In contrast to the procedure above, the slope of the S-N curves is assumed to be of a constant value m = 3 for structural details subjected to normal stresses. Then, the second parameter of the regression line for 50% survival probability (here denoted as $\hat{C}$) can be derived using Equation (4).

$$\log \hat{C} = \frac{1}{n}(\sum \log N_i + m \cdot \sum \log \Delta\sigma_i). \tag{11}$$

The standard deviation s in terms of log N is given by the equation

$$s = \sqrt{\frac{1}{n-1}(\sum \log N_i - (\log \hat{C} - m \cdot \sum \log \Delta\sigma_i))^2}. \tag{12}$$

To derive characteristic values with 95% survival probability, the factor k_n according to [33] may be used. The values of k_n factors are obtained from the prediction method of

fractile estimation [37] depending on whether the standard deviation s (or the coefficient of variation V_x) is known or unknown. Then, the characteristic value of the intercept $\log C_k$ is defined by the equation

$$\log C_k = \log \hat{C} - k_n \cdot s. \tag{13}$$

Finally, the characteristic value $\Delta\sigma_C$ of the fatigue strength at 2×10^6 stress cycles amounts to

$$\log \Delta\sigma_C = \frac{\log 2 \times 10^6 - \log C_k}{-m} \Rightarrow \Delta\sigma_C = 10^{\log \Delta\sigma_C}. \tag{14}$$

Applying this procedure with the value of factor k_n = 1.92 for a number of samples n = 10 and the unknown value of V_x from table D.1 in [33] and using the data in Table 1, the parameter $\log \hat{C}$ takes on a value 12.35, and the characteristic value of stress range is $\Delta\sigma_C$ = 85.6 MPa. The graphic evaluation of the fatigue test results is shown in Figure 17.

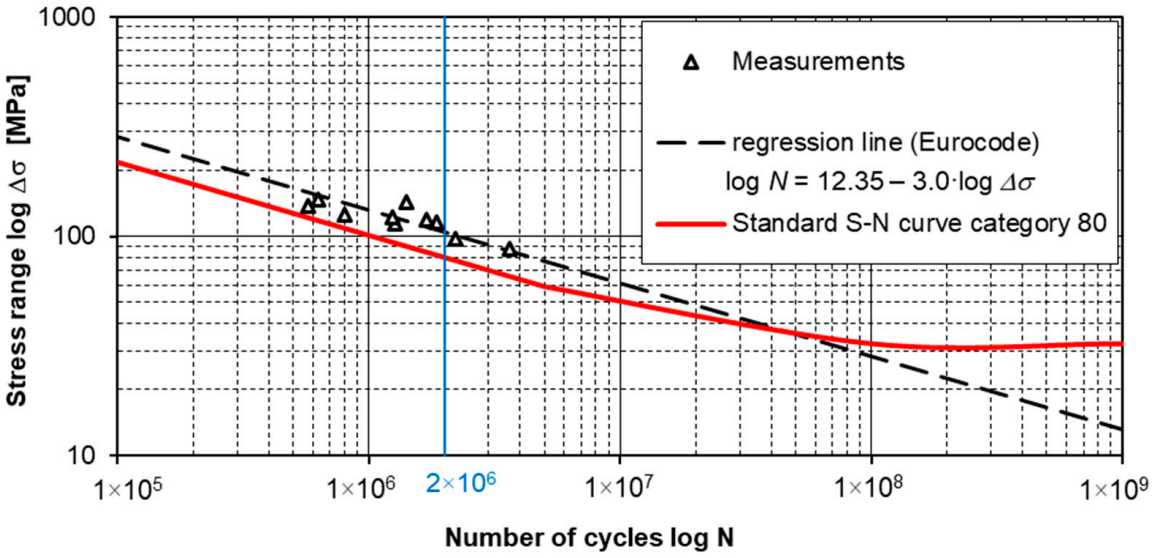

Figure 17. Results of fatigue tests and characteristic S-N curve for the stringer-to-cross-girder connection.

Both the procedures for processing the fatigue test data provide very similar results, which is understandable since both are based on the same mathematical–statistical principles. However, the procedure according to the original Slovak standard [32] enables the determination of the slope of the S-N curve. The results of this procedure confirmed the validity of the assumption of the slope of the S-N curve obtained by the value m = 3 even for the investigated riveted detail. Based on the calculated characteristic values of the stress range $\Delta\sigma_C$ corresponding to 2×10^6 stress cycles, the investigated detail of the stringer-to-cross-girder connection can be classified, in accordance with [18], to the category 80 with characteristic fatigue strength $\Delta\sigma_C$ = 80 MPa.

4. Conclusions

The article deals with the analysis of a typical construction detail of old steel riveted bridges with member bridge decks, namely, the connection of the stringer to the cross girder where a fatigue crack growing in the stringer web quite often occurs (Figure 1). The main conclusions of the performed numerical and experimental analyses are as follows:

- The results of the performed analyses confirmed the connection between the appearance of fatigue cracks in this detail and the actual bending stiffness of the stringer-to-cross-girder connection, which used to be neglected at the time of the design of these bridges.
- Although from the point of view of the rigidity of this joint, the mutual connection of the flanges of the stringers connecting to the cross girder is of fundamental importance; even the joint realised only by connecting the webs of the stringers and the cross girder

using connecting angles shows a certain bending stiffness. This can be safely neglected when assessing the bending resistance of the stringer in the middle of its span.
- The real stiffness of such a connection causes a more complex stress state in its vicinity than can be provided by simple theoretical models, such as a hinged connection or a rigid connection. In this context, the connection strengthening by end haunches at the lower flange of the stringer proved to be very important.
- In cases where it is necessary to carefully consider the stress in the joint area, it is recommended to model this joint more accurately, for example, by using shell elements when processing the FEM model of the superstructure.
- The fatigue tests of this structural detail were performed on specially prepared laboratory test specimens.
- Based on the linear regression analysis of the obtained test results, the fatigue category of the investigated detail was determined, given by the fatigue strength value $\Delta\sigma_C$ = 80 MPa corresponding to the number of load cycles of 2×10^6.
- This detail category can be used to verify the fatigue resistance of old riveted bridges according to European standards.

Author Contributions: Numerical analyses within the theoretical study focused on the stiffness of the investigated connection—J.J.; processing of the results of experimental measurements on the real bridge structure—J.G.; numerical analysis of the bridge superstructure—J.G.; preparation, realization and processing of the results of fatigue tests of the observed detail—J.J., J.G. and J.V.; numerical analyses of the tested fatigue detail—J.J.; evaluation of the results of fatigue tests and determination of the fatigue detail category—J.G.;. supervision and coordination of individual works—J.V.; ensuring project administration—J.V.; writing—preparation of the original draft—J.G. and J.J.; writing—review and editing—J.V. All authors have read and agreed to the published version of the manuscript.

Funding: This research was supported by the Scientific Grant Agency of the Slovak Republic under project 1/0623/21 "Analysis of details and failures of railway bridges steel superstructures".

Institutional Review Board Statement: Not applicable.

Informed Consent Statement: Not applicable.

Data Availability Statement: Data is contained within the doctoral thesis that is available in Central register of final and qualifying theses (in Slovak, https://crzp.cvtisr.sk/, (accessed on 5 January 2022)).

Conflicts of Interest: The authors declare no conflict of interest.

References

1. James, G. Analysis of Traffic Load Effects on Railway Bridges. Ph.D. Thesis, Structural Engineering Division Royal Institute of Technology, Stockholm, Sweden, 2003.
2. Imam, B.; Salter, P.A. Historical load effects on fatigue of metallic railway bridges. *Proc. Inst. Civil Eng.-Bridge Eng.* **2018**, *171*, 49–62.
3. Frøseth, G.T.; Rönnquist, A. Evolution of load conditions in the Norwegian railway network and imprecision of historic railway load data. *Struct. Infrastruct. Eng.* **2019**, *15*, 152–169. [CrossRef]
4. Ižvolt, L.; Šmalo, M. Historical Development and Applications of Unconventional Structure of Railway Superstructure of the Railway Infrastructure of the Slovak Republic. *Civ. Environ. Eng.* **2014**, *10*, 79–94. [CrossRef]
5. Garbarova, M.; Strezova, M. The Trend Analysis of Transport Development in Slovak Republic. *Procedia Econ. Finance* **2015**, *26*, 584–591. [CrossRef]
6. Pipinato, A.; Pellegrino, C.; Modena, C. Residual life of historic riveted steel bridges: An analytical approach. *Proc. Inst. Civ. Eng.-Bridge Eng.* **2014**, *167*, 17–32. [CrossRef]
7. Odrobiňák, J.; Hlinka, R. Degradation of Steel Footbridges with Neglected Inspection and Maintenance. *Procedia Eng.* **2016**, *156*, 304–311. [CrossRef]
8. Koteš, P.; Brodňan, M.; Bahleda, F. Diagnostics of Corrosion on a Real Bridge Structure. *Adv. Mater. Sci. Eng.* **2016**, *2016*, 1–10. [CrossRef]
9. Odrobiňák, J.; Gocál, J. Experimental measurement of structural steel corrosion. *Procedia Struct. Integr.* **2018**, *13*, 1947–1954. [CrossRef]
10. Gocál, J.; Odrobiňák, J. On the Influence of Corrosion on the Load-Carrying Capacity of Old Riveted Bridges. *Materials* **2020**, *13*, 717. [CrossRef]

11. Štecák, R. The Influence of corrosion on the stresses in members of open deck railway bridges. *IOP Conf. Ser. Mater. Sci. Eng.* **2019**, *566*, 012031. [CrossRef]
12. Macho, M.; Ryjáček, P.; e Matos, J.A.C. The residual lifetime of steel bridges under the action of fatigue and corrosion effects. *IOP Conf. Ser. Mater. Sci. Eng.* **2018**, *419*, 012026. [CrossRef]
13. Imam, B.; Righiniotis, T.D.; Chryssanthopoulos, M.K. Connection fixity effects on stress histories in riveted rail bridges. In Proceedings of the 2nd International Conference on Bridge Maintenance, Safety and Management IABMAS'04, Kyoto, Japan, 19–22 October 2004.
14. Al-Emrani, M. Fatigue Performance of Stringer-to-Floor-Beam Connections in Riveted Railway Bridges. *J. Bridg. Eng.* **2005**, *10*, 179–185. [CrossRef]
15. SCIA Engineer. Structural Analysis Software. Available online: https://www.scia.net/en (accessed on 5 January 2022).
16. Fisher, J.W. *Bridge Fatigue Guide. Design and Details*; American Institute of Steel Construction: Chicago, IL, USA, 1977.
17. Keating, P.B.; Fisher, J.W. *Evaluation of Fatigue Tests and Design Criteria on Welded Details*; National Cooperative Highway Research Program report 286; Transportation Research Board: Washington, DC, USA, 1986.
18. *EN 1993-1-9*; Eurocode 3: Design of Steel Structures—Part 1.9: Fatigue. CEN: Brussels, Belgium, 2003.
19. Adamson, D.E.J.; Kulak, G.L. Fatigue Tests of Riveted Bridge Girders; Structural Engineering Report, No. 210. Master's Thesis, University of Alberta, Edmonton, AB, Canada, 1995.
20. Matar, E.B. Evaluation of Fatigue Category of Riveted Steel Bridge Connections. *Struct. Eng. Int.* **2007**, *17*, 72–78. [CrossRef]
21. Cremona, C. *Improved Assessment Methods for Static and Fatigue Resistance of Old Steel Railway Bridges*; Report from the Integrated Research Project "Sustainable Bridges—Assessment for Future Traffic Demands and Longer Lives" Funded by the European Commission within 6th Framework Programme; European Commission: Brussels, Belgium, 2007.
22. Larsson, T. Fatigue Assessment of Riveted Bridges. Ph.D. Thesis, Luleå University of Technology, Luleå, Sweden, 2009.
23. Taras, A.; Greiner, R. Development and Application of a Fatigue Class Catalogue for Riveted Bridge Components. *Struct. Eng. Int.* **2010**, *20*, 91–103. [CrossRef]
24. Macho, M.; Ryjáček, P.; Matos, J. Fatigue Life Analysis of Steel Riveted Rail Bridges Affected by Corrosion. *Struct. Eng. Int.* **2019**, *29*, 551–562. [CrossRef]
25. Lehner, P.; Krejsa, M.; Pařenica, P.; Křivý, V.; Brožovský, J. Fatigue damage analysis of a riveted steel overhead crane support truss. *Int. J. Fatigue* **2019**, *128*, 105190. [CrossRef]
26. Pipinato, A.; Pellegrino, C.; Bursi, O.; Modena, C. High-cycle fatigue behavior of riveted connections for railway metal bridges. *J. Constr. Steel Res.* **2009**, *65*, 2167–2175. [CrossRef]
27. Pipinato, A.; Pellegrino, C.; Modena, C. Assessment procedure and rehabilitation criteria for the riveted railway Adige Bridge. *Struct. Infrastruct. Eng.* **2012**, *8*, 747–764. [CrossRef]
28. Haghani, R.; Al-Emrani, M.; Heshmati, M. Fatigue-Prone Details in Steel Bridges. *Buildings* **2012**, *2*, 456–476. [CrossRef]
29. Kroyer, R.M.; Taras, A. Ultimate and fatigue limit states of existing steel railway bridges—LRFD with historical steel products and connection types. *Steel Constr.* **2023**, *16*. [CrossRef]
30. Goodman, J. *Mechanics Applied to Engineering*; Longman, Green & Company: London, UK, 1899.
31. Sivák, P.; Ostertagová, E. Evaluation of Fatigue Tests by Means of Mathematical Statistics. *Procedia Eng.* **2012**, *48*, 636–642. [CrossRef]
32. *STN 73 1401*; Design of Steel Structures. SUTN: Bratislava, Slovakia, 1998.
33. *EN 1990*; Basis of Structural Design. CEN: Brussels, Belgium, 2003.
34. Brozetti, H.; Hirt, M.; Ryan, I.; Sedlacek, G.; Smith, I. *Background Information on Fatigue Design Rules—Statistical Evaluation*; Chapter 9—Document 9.01, 1st draft, Eurocode 3—Editorial Group; ECCS: Brussels, Belgium, 1998.
35. Bartsch, H.; Drebenstedt, K.; Seyfried, B.; Feldmann, M.; Kuhlmann, U.; Ummenhofer, T. Analysis of fatigue test data to reassess EN 1993-1-9 detail categories. *Steel Constr.* **2020**, *13*, 280–293. [CrossRef]
36. Drebenstedt, K.; Kuhlmann, U. Re-evaluation and extension of fatigue test data for welded attachments and butt joints. *ce/papers* **2021**, *4*, 1160–1167. [CrossRef]
37. Leonardo Da Vinci Pilot Project CZ/02/B/F/PP-134007. *Implementation of Eurocodes, Handbook 2, Reliability Backgrounds*; Guide to the Basis of Structural Reliability and Risk Engineering Related to Eurocodes, Supplemented by Practical Examples; European Commission: Prague, Czech Republic, 2005.